OVERVIEW OF SOME FEEDBACK- & CONTROL SYSTEMS AT SYNCHROTRON SOLEIL

C. Engblom*, F. Alves, F. Blache, D. Corruble, A. Dawiec, M. Diop, N. Hubert,
S. Kubsky, F. Langlois, P. Marchand, N. Jobert, G. Renaud, Y.M. Abiven
Synchrotron SOLEIL, Saint-Aubin, France
T. Stankevic, MAXIV, Lund, Sweden

Abstract

This paper gives an overview of some feedback & control systems at Synchrotron SOLEIL that are in use or in development today. Beam stability is crucial and adressed in all SOLEIL aspects; Fast Orbit Feedback is a multi-input multi-output control system made to stabilize beam position perturbations in the low- & high frequency band. In addition, active RF cavities are used to maintain stable beam energy & spread as well as keeping electron density even throughout the storage ring. Beam stability also comes from feedforward non-linear control in particle trajectory compensation on both sides of electromagnetic undulators. On some beamlines, multi-actuator piezos or pneumatics are used to regulate photon flux to keep within detector operating range; a method to maximize the photon flux while still keeping below detector damage thresholds. Currently in development & at the sample stage level, the Nanoprobe Project collaboration (MAXIV & SOLEIL) focuses on sample stabilization during step- & fly- scans which is realized through multi-axis nano-positioning with high- & low- frequency closed-loop control implementing interferometer feedback &/or compensation tables.

INTRODUCTION

For the past couple of years Synchrotron SOLEIL has, in a collaboration project with MAXIV, been constructing an endstation prototype capable of 2D- and 3D tomography scans on the nanometric scale. Such a project not only relies on passive thermal stability and vibration but also on feedback systems. These systems are not only crucial in the endstation setup but also relies on the stability provided by a series of feedback systems that resides in the storage ring, entry and exits of insertion devices, radiofrequency systems and photon flux regulating devices to provide stable photon beam positioning and flux to beamline endstations. In long beamlines, such as Nanoscopium [1] in Synchrotron SOLEIL or NanoMax [2] in MAXIV, endstations particularly specialize in scanning x-ray microscopy on the nano-scale.

As such, this paper provides an overview of some of the existing feedback systems in Synchrotron SOLEIL with a focus on the progress of the Nanoprobe project.

BEAM ORBIT STABILITY SYSTEM

Stable photon flux to the beamlines is in part provided by ensuring electron beam position and angle stability in the storage ring. For this reason the Global Orbit Feedback System (GOFB) is necessary against environment perturbations in the long term (hours to a day, ex: thermal effects, sun & moon tides), medium term (seconds to minutes, ex: moving crane, insertion devices), and short term (less than a second, ex: booster cycling operations, ground vibrations) [3]. The frequency spectrum of the noise at SOLEIL Synchrotron has been shown to reside in the range from DC→150 Hz [3].

The GOFB correction algorithm is based on Singular Value Decomposition (SVD) where an inverse response matrix, R^{-1}, together with the orbit error, ΔU_{BPMi}, is used to calculate the correction currents, ΔI_{corrj} [3]. Multiplication is shown in Eq. 1, the matrix dimensions of R^{-1} are here denoted as $M \times N$ and directly corresponds to the number of Beam Position Monitors, N, and number of current actuators, M.

$$\begin{bmatrix} \Delta I_{corr\ j} \\ \Delta I_{corr\ j+1} \\ \vdots \\ \Delta I_{corr\ j+M} \end{bmatrix} = R^{-1} \cdot \begin{bmatrix} \Delta U_{BPM\ i} \\ \Delta U_{BPM\ i+1} \\ \vdots \\ \Delta U_{BPM\ i+N} \end{bmatrix} \quad (1)$$

The GOFB is divided into two systems [3]:

- The Slow Orbit Feedback (SOFB), with correction rate and bandwidth limited to 0.1 Hz
- The Fast Orbit Feedback (FOFB), with correction rate to 10 kHz and efficient up to a few hundred Hz.

The two systems contain their own sets of correctors and can run inpendently of each other. This can cause interference if their control-frequencies are overlapping which is why there are three approaches that can be used [3]:

1. 'Deadband' method (Fig. 1), a frequency deadband is introduced between the two systems guaranteeing complete independency from each other. The issue with this method is that the deadband needs to be sufficiently large and if there are components creating disturbances inside the deadband spectrum they can't be corrected for.
2. 'FOFB only' method (Fig. 2), run the FOFB system alone for all frequencies down to DC. This approach, due to the weakness of fast correctors, have limits on correction amplitudes and might saturate the correctors.
3. 'FOFB/SOFB interaction' method (Fig. 3), the SOFB corrects low-frequency disturbances while predicting

* christer.engblom@synchrotron-soleil.fr

ISBN 978-3-95450-189-2

its next-iteration corrections. It then subtracts the predicted changes from the next-iteration FOFB correction.

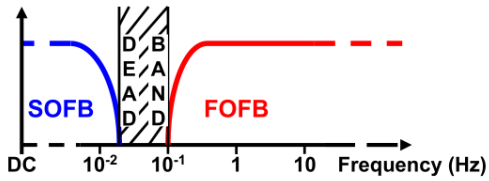

Figure 1: Deadband approach.

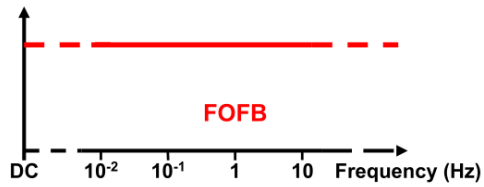

Figure 2: 'FOFB only' approach.

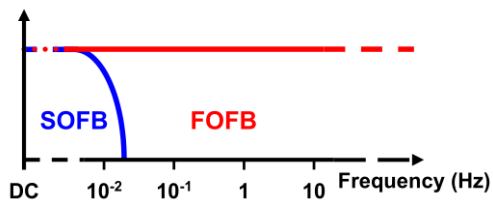

Figure 3: 'FOFB/SOFB interaction' approach.

Status of the GOFB at Synchrotron SOLEIL

SOLEIL is currently using the 'FOFB/SOFB interaction' approach with a DC-download algorithm which allows it to do corrections in the frequency domain from DC → 250 Hz [3]. Two different sets of correctors are being used: strong iron-core correctors for SOFB (bandwidth limitations), and low-inductance correctors for FOFB (high bandwidth, but with lower degree of corrections) [3]. From these, SOLEIL can benefit from having the fast correction without saturation.

The GOFB has been using in total 122 e-BPM as sensors and has been doing so since 2008 [4]. Since 2013 however, XBPMs have been included as additional sensors in the correction algorithm; since the XBPMs are situated in the front-end, they provide a better position angular measurement of the beam [4]. They are implemented into the SVD SOFB system and have been able to improve peak-to-peak position stability of the photon beam by a factor of 1.3 – 3 [4].

STORAGE RING RF SYSTEMS

In the SOLEIL storage ring the RF system provides the power of 600 kW and the RF voltage of 3-4 MV at 352 MHz, which are required to store 500 mA at the nominal energy of 2.75 GeV. This is achieved using 2 cryomodules, each containing a pair of superconducting cavities. Each of the four cavities is powered by a 180 kW solid state amplifier and the two cryomodules are supplied with liquid helium at 4.5 K from a single cryogenic station [5].

Figure 4 shows a block diagram of one of the four low level RF (LLRF) systems which allows to control the cavity accelerating voltage with the required level of stability in terms of frequency, amplitude and phase. The amplitude loop (Fig. 4, orange) regulates the amplitude of the cavity accelerating voltage by comparing the signal from a cavity pickup with a reference voltage; the error signal acts on a variable attenuator through a PID. The phase loop (Fig. 4, green) maintains constant the phase between the RF generator and the cavity voltage by driving a phase shifter with the error signal from a phase comparator through a PID. Each cavity has its own frequency tuner, a mechanism driven by a linear stepper motor, which changes the cavity length and therefore its resonant frequency. The motor is controlled by the error signal from the tuning loop (Fig. 4, in grey) and a SOLEIL standard ControlBox unit (Fig. 5). The fast direct RF feedback (Fig. 4, in red), which reinjects a sample of the cavity RF voltage at the input of the amplification chain, is aimed at coping with the Robinson instability at high beam loading. The achieved stability is 0.1% in amplitude and 0.1° in phase.

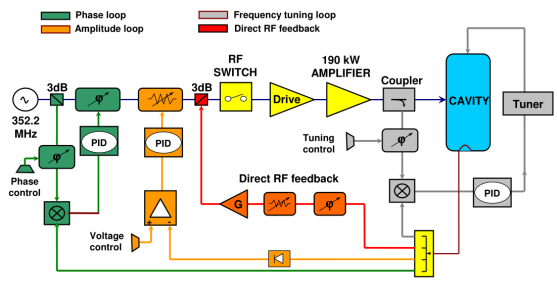

Figure 4: Low-Level Control scheme of an RF cavity.

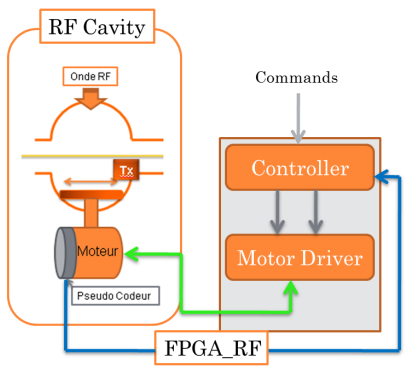

Figure 5: RF cavity motor control scheme. The stepper motor is controlled by a SOLEIL ControlBox using pseudo encoder feedback (in the form of an analog signal) from an FPGA system.

In the Booster, a 5-cell normal conducting copper cavity, powered with a 35 kW solid state amplifier, provides an RF

ISBN 978-3-95450-189-2

voltage of 1 MV at 352 MHz. The LLRF system is similar to that of the storage ring, but there is no need for direct RF feedback as the beam current is much lower. Although we have developed a prototype of digital FPGA-based LLRF system, which could achieve similar performance, we are still using our original fully analog LLRF system [6].

TRAJECTORY COMPENSATION IN ELECTROMAGNETIC INSERTION DEVICES

In order to correct for close orbit distortions (COD) in electromagnetic insertion devices (ID), a fast electromagnetic field variation in the correctors (at entry/exit of the ID) and in the ID is needed [7]. Previous control systems used high-level software for control via Profibus which had limitations on COD synchronization and electromagnetic switching rates [7]. In order to improve this performance, a new control system based on a set of boards ("SPI BOARD PACKAGE", developed at SOLEIL) was implemented [7]. Figure 6 shows the control architecture using the SPICONTROLLER and SPIDAC configuration, a low-level microcontroller which in this case manages the feedforward compensation in the form of look-up tables. These tables, derived from position measurements from the ID, generate corrections analog signals (for the correctors and main ID coil) in function of main coil current [7]. A TANGO high-level software is used to configure the SPICONTROLLER [7].

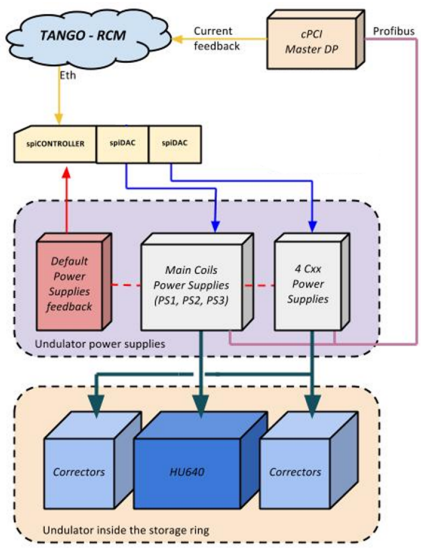

Figure 6: Control architecture of HU640 insertion device control with SPIBOARDS package.

Figure 7 shows the results from using the SPICONTROLLER setup on a HU256 undulator: the COD were reduced by as much as a factor of 3 down to 8 µm [7].

FAST ATTENUATION DEVICE

The Fast Attenuation (FastAtt) device was originally implemented for the SIXS beamline in 2012 in order to regulate

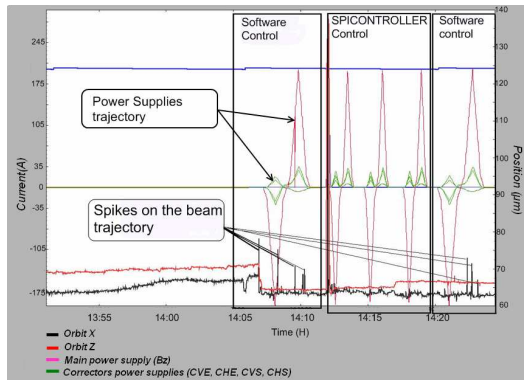

Figure 7: The difference between old and new control system of HU256 undulators. Beam trajectory spikes are reduced from about 25 µm down to 8 µm using the new control system. The center of the figure shows the power supply trajectory and in the bottom is the machine beam orbit. In the graph, the old control system is identified by software control and the new one by SPICONTROLLER control.

the photon flux to keep below detector damage thresholds and keep within their optimal operating range [8]. The system contains a control unit, here based on a CompactPCI board, and attenuator actuators (See Fig. 8) [8]. The control board measures the mean photon flux from a detector and compares the value with pre-programmed thresholds and makes the necessary actuators adjustments [8]. Depending on the photon detector, two different architectures are possible: a point detector (since 2012) or an XPAD 2D-sensor [9] (since 2015). Both systems are in use depending on the application. In the case of the XPAD- setup (see Fig. 8), an intensity analyser board performs image processing.

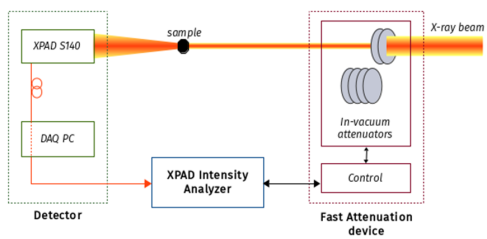

Figure 8: Global architecture of the controlled 2D XPAD attenuation system.

The FastAtt actuators each hold photon filters which are controlled with binary logic that moves each filter independently in and out of the photon beam pathway. Combined control of all actuators then provides for a very high range of beam attenuation. This is particularly useful when performing scans over high photon energy ranges that would normally saturate detectors at certain points, the FastAtt system would simply apply the necessary filtering and avoid detector saturation.

The attenuation reaction time is an important factor as it dtermines how useful the system would be for continuous scans such as Flyscans [10] the pneumatic actuators have shown to have a 150 ms reaction times, and 10ms for piezo

ISBN 978-3-95450-189-2

actuators [8]. Today, the SIXS beamline uses two FastAtt setups: one with pneumatic actuators and another with piezo driven ones.

NANOPROBE PROJECT

The Nanoprobe Project was initiated to deliver a scanning hard X-ray Fresnel Zone Plate (FZP)- based microscope with a scanning sample stage for long beamline endstations in Nanoscopium in Synchrotron SOLEIL and NanoMAX in MAXIV. Some of the challenging aspects were to produce nanometric precision coupled with millimeter range and 360° sample movement and rotation, while also providing Flyscans [10] and long-term stability. Figure 9 shows a schematic of the endstation setup with beam focusing stages (Fresnel Zone Plates, Central Stop, Order Sorting Aperture) and Sample Stage.

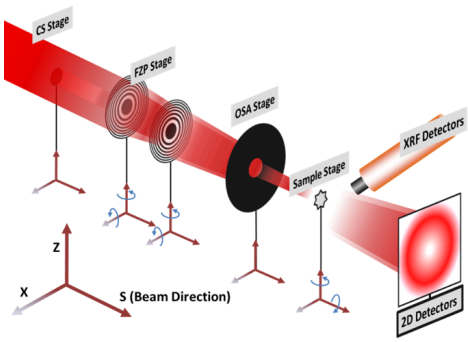

Figure 9: End-station scheme of stages and detectors and their orientation in respect to the beam.

The approach was to, in addition of providing a stable environment in terms of vibration and temperature, to construct a modular and stacked design with an interferometric feedback system and the possibility of using position compensation (in feedforward control) to diminish repeatable errors of the linear and rotation stages.

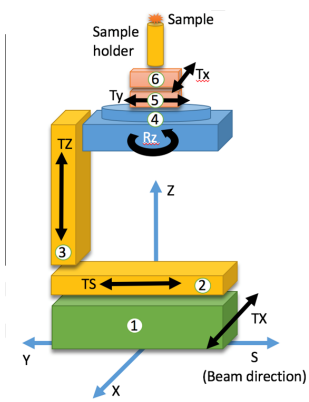

Figure 10: Sample stage schematic setup.

Figure 10 gives a schematic example of how the sample stage was built; a stacked design with (X, S, Z, Rz) from numbers 1-4 and eccentricity- correction stages numbered on 5-6. The sample holder is a cylindrical reflector, providing feedback for interferometer readings.

Control Schemes

Control for the different stages was achieved by utilizing two main schemes; one that is used for fast and dynamic control (see Fig. 11) while the other one provides for slow point-to-point static positioning (see Fig. 12). These control schemes are cascaded with an inner loop (usually higher frequency) residing in the actuator driver, and an outer loop containing either a Delta Tau or a Galil as superior controllers. Due to the stacked and modular design, the same control scheme as depicted in Fig. 11 can be used for simultaneous motion of all axes within the sample stage without the need of resorting to kinematic conversions. The scheme depicted in Fig. 12 was used in the beam focusing stages such as the FZP stage. Positioning errors in the form of parasitic movements, thermal drifts, and vibrations were still evident at the nanometric level which were diminished by two main approaches:

1. *Position Compensation:* repeatable errors were measured and compensated for in a feedforward manner. This approach needs interferometry for building the compensation table. Position compensation can be linked between axes, effectively creating compensation in several degrees of freedom.

2. *Interferometry Closed-Loop:* closed-loop control using interferometry at the Delta Tau/Galil controller level: interferometry feedback on the sample stage is done very close to the sample (a few mm) and it is possible to correct for errors at the same frequency in which they are perceived. Assuming a perfect reflector, any perceived error is the actual position error. If the reflector is not a perfect cylinder, its shape needs to be determined in an independent measurement. The shape is then used for mapping on which position compensation on the interferometry signal can be done.

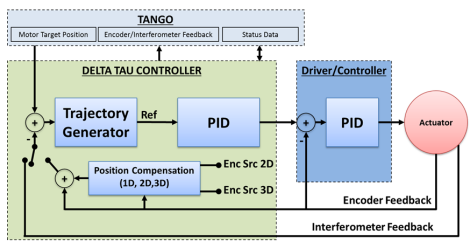

Figure 11: Sample stage control scheme with a Delta Tau Controller.

Sample Stage Scan Results

2D- scanning performance with continuous and stepping motion along the XZ-axes were tested using the different control schemes to diminish positioning errors. In Fig. 13 the motion errors are shown during 1×1 µm scans with continuous Flyscan [10] acquisition in the X-axis while performing

ISBN 978-3-95450-189-2

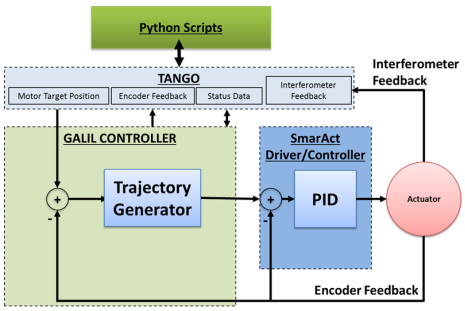

Figure 12: FZP stage control scheme with a Galil controller.

step-scanning on the Z-axis; here closed-loop with direct feedback from the interferometers was done yielding X-error of 8.2 nm FWHM and 2.8 nm FWHM on the Z-error. The errors were calculated by subtracting the reference trajectory from the displacements measured using interferometry.

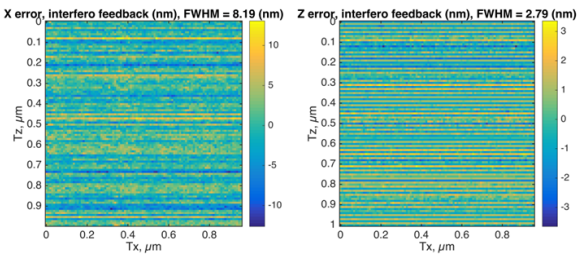

Figure 13: Positioning errors during 1×1 µm 2D continuous scans. Continuous scans were done along the X-axis and Z-Axis performed stepscans in 10 nm increments. Correction of X and Z errors by using closed-loop interferometry feedback. Color bar is in nanometers.

FZP Active Stabilization Results

An active closed-loop stabilization with interferometers (as depicted in Fig. 12) was implemented that calculated the drift of the FZP holder from the interferometry measurements and kept it within a set threshold by commanding the corresponding positioner movements. Multi-axes control with kinematic equations was used and programmed in a python script that acted through a TANGO device. The control frequency was about 1 Hz. As seen in Fig. 14, the FZP position kept within approximately 5 nm FWHM.

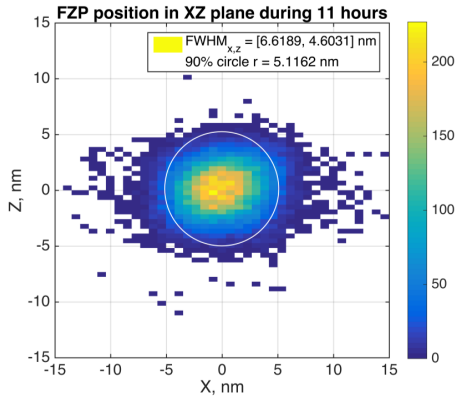

Figure 14: 2D histogram of the FZP XZ-position during 11 hours of active stabilization. The FWHM is 6.6 nm in X and 4.6 nm in Z. 90% of the time the FZP position is within $r = 5.1$ nm circle.

REFERENCES

[1] A. Somogyi *et al.*, "Status of the Nanoscopium scanning hard x-ray nanoprobe beamline of synchrotron SOLEIL", in *11th Int. Conf. on X-ray Microscopy (XRM2012)*, Shanghai, China, Aug. 2012.

[2] U. Johansson *et al.*, "NanoMAX: a hard x-ray nanoprobe beamline at MAX IV", in *Proc. of SPIE Vol. 8851 88510L-9*, 2013.

[3] N. Hubert, L. Cassinari, J-C. Denard, A. Nadji, L. Nadolski, "Global orbit feedback systems down to DC using fast and slow correctors", in *Proc. 9th European Workshop on Beam Diagnostics and Instrumentation for Particle Accelerators (DIPAC'09)*, Basel, Switzerland, May 2009, paper MOOC01, pp.27-31.

[4] N. Hubert *et al.*, "SOLEIL beam stability status", in *Proc. 4th Int. Particle Accelerator Conf. (IPAC'13)*, Shanghai, China, May 2013, paper WEPME001.

[5] P. Marchand *et al.*, "Commissioning of the SOLEIL RF systems", in *Proc. 10th European Particle Accelerator Conf. (EPAC'06)*, Edinburgh, Scotland, June 2006, paper MOPCH142, pp.384-386.

[6] M. Diop *et al.*, "Low level RF system development for SOLEIL" in *Proc. 10th European Particle Accelerator Conf. (EPAC'06)*, Edinburgh, Scotland, June 2006, paper TUPCH186, pp.1447-1449.

[7] Y.M. Abiven *et al.*, "Analogue feedforward for SOLEIL electromagnetic insertion devices", in *Proc. 11th Int. Conf. on Synchrotron Radiation Instrumentation (SRI2012)*, Lyons, France, July 2012, pp.201-204.

[8] G. Renaud *et al.*, "Beamline fast and automatic attenuation system for x-ray detectors at Synchrotron SOLEIL", in *Proc. 11th Int. Conf. on Synchrotron Radiation Instrumentation (SRI2012)*, Lyon, France, July 2012.

[9] S. Basolo *et al.*, "XPAD: pixel detector for material sciences", in *IEEE Transactions on Nuclear Science, Institute of Electrical and Electronics Engineers*, 2005, 52, pp.1994-1998.

[10] N. Leclerq *et al.*, "Flyscan: A fast and multi-technique data acquisition platform for the SOLEIL beamlines", in *Proc. 15th of Int. Conf. on Accelerator & Large Experimental Physics Control Systems (ICALEPCS'15)*, Melbourne, Australia, Oct. 2015, paper WEPGF056, pp.826-829.

ISBN 978-3-95450-189-2